# Particle decay of $^{12}$Be excited states

R. J. Charity, S. A. Komarov, and L. G. Sobotka
*Departments of Chemistry and Physics, Washington University, St. Louis, Missouri 63130, USA*

J. Clifford, D. Bazin, A. Gade, Jenny Lee, S. M. Lukyanov,* W. G. Lynch, M. Mocko, S. P. Lobastov,* A. M. Rogers, A. Sanetullaev, M. B. Tsang, and M. S. Wallace
*National Superconducting Cyclotron Laboratory and Department of Physics and Astronomy, Michigan State University, East Lansing, Michigan 48824, USA*

S. Hudan and C. Metelko
*Department of Chemistry and Indiana University Cyclotron Facility, Indiana University, Bloomington, Indiana 47405, USA*

M. A. Famiano and A. H. Wuosmaa
*Department of Physics, Western Michigan University, Kalamazoo, Michigan 49008, USA*

M. J. van Goethem
*Kernfysisch Versneller Institut, NL-9747 AA Groningen, The Netherlands*
(Received 22 June 2007; published 17 December 2007)

The breakup of $E/A = 50$ MeV $^{12}$Be fragments following inelastic scattering off of hydrogen and carbon target nuclei has been studied. The breakup channels $\alpha$+$^{8}$He, $^{6}$He+$^{6}$He, $t + {}^{9}$Li, and $p$+$^{11}$Li were observed. Two doublets at excitation energies of 12.8 and 15.5 MeV were found for the $\alpha$+$^{8}$He channel. A low-energy shoulder in the excitation-energy spectra at 10.2 MeV indicates one or more additional states. This work could not confirm the presence of $^{6}$He-$^{6}$He rotational structure reported by Freer *et al.* [Phys. Rev. C **63,** 034301(2001)], although possible peaks at excitation energies of 13.5 and 14.5 MeV were found for $^{6}$He+$^{6}$He decay. Significant structure is observed in the excitation-energy spectrum for $p$+$^{11}$Li at 25–30 MeV which maybe associated with $T = 3$ analog states.

DOI: 10.1103/PhysRevC.76.064313 PACS number(s): 21.60.Gx, 25.60.−t, 25.70.Ef, 27.20.+n

## I. INTRODUCTION

The structure of light nuclei is known to be associated with strong alpha-particle clustering [1]. This is true not only for $^{8}$Be and $^{12}$C, but also when additional nucleons are added to these multi-alpha-particle nuclei. For example, $^{9}$Be can be modelled as a three-body system composed of a core of two $\alpha$ particles and a valance neutron [2–4]. An analogy to molecular systems, the simplest being $H_2^+$, is strong as the core $\alpha$-$\alpha$ interaction is repulsive and the valence neutron (playing the role of the electron in $H_2^+$) provides the binding. The analogy can be taken further as excited states have $\sigma$ and $\pi$-like symmetries [5]. The wavefunctions and density distributions of $\sigma$-like states are axially symmetric about the $\alpha$-$\alpha$ axis while the $\pi$-like have a nodal plane containing the $\alpha$-$\alpha$ axis.

Molecular states associated with two "valence" neutrons are also predicted for $^{10}$Be [5]. Two rotational bands based on exited $0^+$ and $1^-$ states have been observed [4]. Their moments of inertia are significantly larger than the ground-state rotational band suggesting molecular configurations. The $4^+$ members of the first band particle decays to the $\alpha$-$^{6}$He exit channel indicating it has a strong cluster structure [6].

Molecular structures have also been predicted for $^{12}$Be [5,7,8]. In experiments where $^{12}$Be beams were excited via inelastic scattering, evidence has been presented for molecular states. Korsheninnikov *et al.* [9] detected recoil protons following $^{12}$Be+$p$ scattering and identified narrow $^{12}$Be states at 8.6, 10, and ∼14 MeV. It was argued that the widths of these states are too narrow for neutron decay and thus they may have strong cluster structure and decay by helium emission. Freer *et al.* [10,11] have found evidence for $^{12}$Be levels which decay through the $^{6}$He-$^{6}$He and $\alpha$-$^{8}$He exit channels after scattering off carbon and $(CH_2)_n$ targets. The $^{6}$He-$^{6}$He breakup states were tentatively assigned spins of 4, 6, and 8 suggesting these are part of a rotational band. Saito *et al.* [12] present evidence for $^{6}$He-$^{6}$He breakup states following inelastic scattering from $^{4}$He. The states at 10.9 and 11.3 MeV were assigned spins of 0 and 2, respectively. Combined with results of Freer *et al.*, a rotational band with states of spin from 0 to 8 can be inferred with a large moment of inertia consistent with two touching $^{6}$He nuclei in a molecular configuration.

$^{6}$He-$^{6}$He breakup states were also reported following $^{12}$C ($^{14}$Be,$^{12}$Be) two-neutron removal reaction [13]. A state at 11.8 MeV level was tentatively assigned spin 0. In the three-neutron transfer reaction $^{9}$Be($^{15}$N,$^{12}$N)$^{12}$Be, Bohlen *et al.* report peaks at 10.7, 14.6, 19.2, and 21.7 MeV which they speculate are part of a molecular band [14]. However, the

*On leave from Flerov Laboratory of Nuclear Reactions, Joint Institute for Nuclear Research, RU-141980 Dubna, Moscow region, Russian Federation.

 

TABLE I. Breakup $Q$-values for all possible binary breakup channels.

| channel | $Q$ [MeV] |
|---|---|
| $n$-$^{11}$Be | −3.17 |
| $\alpha$-$^{8}$He | −8.95 |
| $^{6}$He-$^{6}$He | −10.11 |
| $t$-$^{9}$Li | −14.82 |
| $p$-$^{11}$Li | −23.00 |

decay of these excited $^{12}$Be fragments was not investigated. A more recent search with the $^{10}$Be($^{14}$C,$^{12}$Be) two-neutron transfer reaction failed to see any evidence for $^{6}$He-$^{6}$He or $\alpha$-$^{8}$He breakup states [15].

All these previous studies suffer from limited statistics. Thus, it is important to try and confirm the existence of these levels and their spin assignments to make a solid case for molecular structure in $^{12}$Be. In this work we present new experimental data using $^{12}$Be inelastic scattering. This work is similar to the study of Freer *et al.* in that both targets of polyethylene $(CH_2)_n$ and carbon were employed and that the $^{12}$Be breakup states are identified from correlations between the decay products. However, it differs in using a higher beam energy of $E/A = 50$ MeV as compared to 31 MeV in the study of Freer *et al.* In addition to the $\alpha$+$^{8}$He and $^{6}$He+$^{6}$He exit channels, other breakup modes, $t$+$^{9}$Li and $p$+$^{11}$Li are examined. The Q-values for all possible binary-breakup channels are listed in Table I.

## II. EXPERIMENTAL METHOD

A primary beam of $E/A = 120$ MeV $^{18}$O was extracted from the Coupled Cyclotron Facility at the National Superconducting Cyclotron Laboratory at Michigan State University. This beam bombarded a $^{9}$Be target and $^{12}$Be projectile-fragmentation products were selected by the A1900 separator. The secondary $^{12}$Be beam, with intensity of $1 \times 10^5$ s$^{-1}$, purity of 87%, and momentum acceptance of ±0.5%, impinged on targets of polyethylene and $^{12}$C with thicknesses of 1.0 mm and 0.4 mm, respectively, located at the end of the S800 analysis beam line. The beam spot on these targets was approximately 1 cm×2 cm in area. Event-by-event time of flight was used to reject the beam contaminants.

Charged particles produced in the particle decay of excited $^{12}$Be fragments were detected in the HiRA array [16] consisting of 16$E$-$\Delta E$ [Si-CsI(Tl)] telescopes located 60 cm downstream of the target. The telescopes were arranged in four towers of four telescopes each, with two towers on each side of the beam. The angular regions subtended by this array are shown in Fig. 1 covering a zenith-angle range of $2.7^\circ < \theta < 24.8^\circ$. Each telescope consisted of a 1.5 mm thick, double-sided Si strip $\Delta E$ detector followed by a 4 cm thick, CsI(Tl) $E$ detector. The $\Delta E$ detectors are 6.4 cm×6.4 cm in area with the faces divided into 32 strips. Each $E$ detector consisted of four separate CsI(Tl) elements each spanning a quadrant of the preceding Si detector. Signals produced

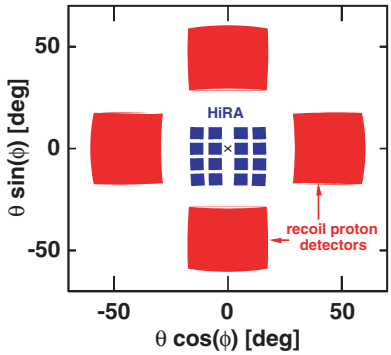


FIG. 1. (Color online) Angular coverage of the detectors in the experiments. The HiRA array was used to detect breakup products of the excited $^{12}$Be fragments. LASSA recoil-proton counters, used to detect recoil-protons following interactions on the hydrogen component of the polyethylene target, are indicated. The cross indicates the beam axis.

in the Si detectors were processed with the HINP16C chip electronics [17].

Recoil protons produced from inelastic scattering interactions of the $^{12}$Be projectile on the hydrogen component of the polyethylene target were detected in 4 LASSA $E$-$\Delta E$ telescopes [18]. Each LASSA telescope contains a 0.5 mm thick, double-sided Si strip $\Delta E$ detector of area 5 cm×5 cm with the faces divided into 16 strips. The $E$ detector for each telescope consists of four 6 cm thick CsI(Tl) crystals, each spanning a quadrant of the preceding Si detector. Figure 1 also indicates the angular coverage of these detectors with zenith angles ranging from $29.4^\circ < \theta < 61.5^\circ$.

Energy calibrations of all Si detectors were obtained from a $^{228}$Th $\alpha$-particle source. The particle-dependent energy calibrations of the CsI(Tl) $E$ detectors were determined using $p, d, t,^{3,4,6,8}$He and $^{6,7,8,9}$Li beams selected using the A1900 separator. Beams were extracted for typically two to six energies for each beam species. These beams were scattered off Au, C, and polyethylene targets into the HiRA and LASSA detectors and calibrations points were fit to linear or second-order polynomial expressions for the energy region of interest. The calibrations for the Li isotopes were found independent of mass number and thus these calibrations were also used for $^{11}$Li fragments.

The resolutions (FWHM) of the Si detectors were ≈80 keV, while the CsI(Tl) detectors had resolutions of ≈4.3%, 2.1%, and 1.8% for $E/A = 50$ MeV protons, $\alpha$ particles and $^{6}$He fragments respectively. The telescopes had excellent isotope resolution as can be seen from the typical $E$-$\Delta E$ plot shown in Fig. 2.

## III. MONTE CARLO SIMULATIONS

Monte Carlo simulations were performed to establish the resolution of the reconstructed excitation energy in the experiment. In these simulations, the interaction depth in the target was chosen randomly and the effects of energy loss [19] and small-angle scattering [20] on the particles as they leave the target were included. The lateral location of the interaction

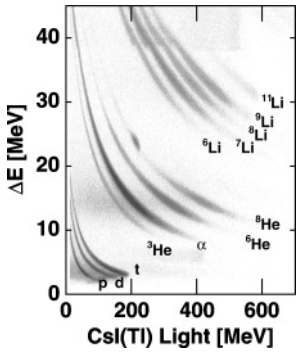


FIG. 2. A typical $E$-$\Delta E$ map of detected particles showing the isotope resolution obtained in the experiment. The energy $E$ measured by the CsI(Tl) light output is calibrated in equivalent proton energy in MeV. Notice the small $^{8}$He beam contaminant.

on the target sampled the measured beam-spot shape. The simulated events were passed through a detector filter and the energy and position resolutions of the detectors were added. Subsequently, the events were analyzed in the same manner as the experimental events. The energy and angular distributions of the reconstructed parent fragments were chosen such that the reconstructed distributions of the "detected" events matched the experimental distributions.

To evaluate the accuracy of these simulations, they were compared to experimental distributions for prominent narrow levels observed in the experiment. The data points in Fig. 3(a) shows the experimental $^{6}$Li excitation-energy distribution determined from $d$-$\alpha$ pairs. The peak is associated with the first excited state of $^{6}$Li ($E^{*} = 2.186$ MeV, $\Gamma = 24$ keV, $J^{\pi} = 3^{+}$). Similarly in Figs. 3(b) and 3(c), peaks associated with $p$-$^{7}$Li and $\alpha$-$^{8}$Li decay of analog states in $^{8}$Be and $^{12}$B are observed. These correspond to the known $E^{*} = 17.64$ MeV, $\Gamma = 10.7$ keV, $J^{\pi} = 1^{+}$ and the $E^{*} = 12.75$ MeV, $\Gamma = 85 \pm 40$ keV, $J^{\pi} = 0^{+}$ states in these respective nuclei. Finally in Fig. 3(d) we see a peak associated the $\alpha$-$^{6}$Li decay of the $E^{*} = 4.774$ MeV, $\Gamma = 8.7$ eV, $J^{\pi} = 3^{+}$ level of $^{10}$B. The $^{12}$B level was produced predominately in the $^{12}$Be$(p, n)^{12}$B reaction, while the other peaks are associated with more complicated interactions with both the hydrogen and carbon components of the polyethylene target. The experimental FWHM are 160, 130, 274, and 90 keV for the $^{6}$Li, $^{8}$Be,$^{12}$B, and $^{10}$B states, respectively, which are significantly larger than their intrinsic values, highlighting the importance of the experimental resolution for these examples.

The thick solid lines in Fig. 3 indicate the predictions of the Monte Carlo simulations. The dashed curves show background contributions which were added to aid in the comparison with data. The simulated results reproduce the experimental distributions quite well. For the $^{10}$B level in Fig. 3(c), the uncertainty in its intrinsic width gives rise to an uncertainty in the predicted peak shape only for the high and low-energy tails. The thin solid curves show the predictions using the upper and lower limits of the experimental uncertainty in the width $\Gamma$ of this $E^{*} = 12.75$ MeV state. Our data are more consistent with the lower limit. These comparisons of the Monte Carlo simulations to data in Fig. 3 give us confidence that they do in fact simulate the response of our apparatus. The most important

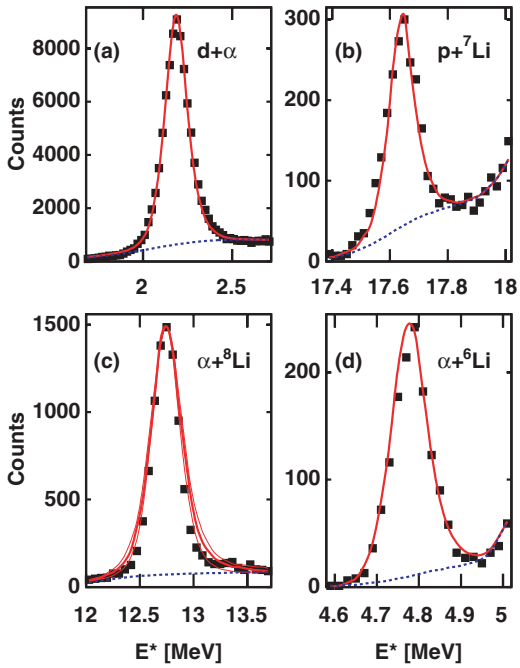


FIG. 3. (Color online) Excitation-energy distributions for (a) $^{6}$Li fragments from $d$-$\alpha$ pairs, (b) $^{8}$Be fragments from $p$-$^{7}$Li pairs, (c) $^{12}$B fragments from $\alpha$-$^{8}$Li pairs, and (d) $^{10}$B fragments from $\alpha$-$^{6}$Li pairs. The data points show the experimental results which can be compared to the thick solid curves indicating the predictions of the Monte Carlo simulations. Background contributions (dashed curves) were added to the simulations to aid in the comparison. In (c), extra thin solid curves are included which correspond to simulations using the upper and lower limits of the experimental intrinsic width of the 12.75 MeV state in $^{12}$B.

contributions to the experimental resolution are the CsI(Tl) energy resolution, the position resolution determined from the width of the Si strips, and small-angle scattering of the decay products in the target.

The large beam-spot size on the target has little effect on the reconstructed excitation energy as the measured relative-angle of the decay products is, to first order, independent of the lateral location on the target. However, the beam-spot size reduced the resolution in reconstructing the parent $^{12}$Be fragment's velocity and scattering angle. The beam-spot size is a larger problem for the recoil-proton detectors which are significantly closer to the target.

## IV. RESULTS

### A. $\alpha$+$^{8}$He decay

For each detected $\alpha$-$^{8}$He pair, their center-of-mass velocity was determined and ascribed to the velocity of the excited $^{12}$Be parent fragment. Joint distributions of the parallel $V_{\parallel}$ and perpendicular $V_{\perp}$components of this velocity are displayed in Figs. 4(a) and 4(b) for the polyethylene and carbon targets, respectively. The dashed curves in both figures indicate the kinematic solutions expected for inelastic scattering on a $^{12}$C target nucleus with a $Q$-value of $-13$ MeV. The solid curve in Fig. 4 gives the equivalent solution loci for interactions

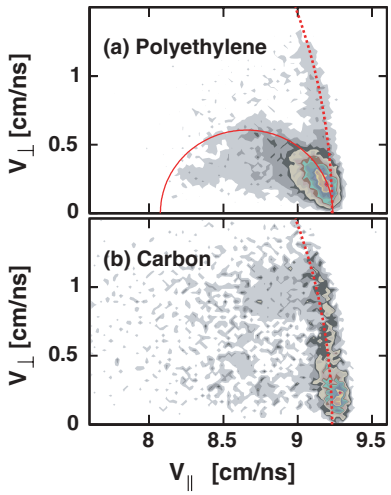


FIG. 4. (Color online) Joint distributions of parallel and perpendicular velocity for $^{12}$Be fragments reconstructed from $\alpha$-$^{8}$He pairs with the (a) polyethylene and (b) carbon targets. The dashed and solid curves indicate the expected loci for scattering off of $^{12}$C and $^{1}$H target nuclei, respectively.

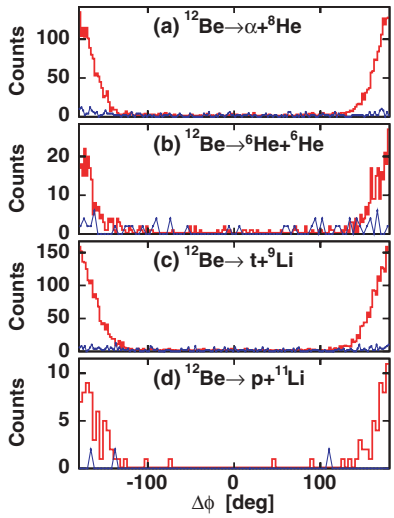


FIG. 5. (Color online) Distributions of relative azimuthal angle between protons detected in the LASSA recoil-proton detectors and the reconstructed $^{12}$Be fragments determined from (a) $\alpha$-$^{8}$He, (b) $^{6}$He-$^{6}$He, (c) $t + {}^{9}$Li, and (d) $p$-$^{11}$Li pairs detected in the HiRA array. The histograms and connected lines were obtained with the polyethylene and carbon targets, respectively.

with a hydrogen nuclei. The experimental results obtained with the carbon target follow the dashed curve confirming the presence of inelastic scattering on $^{12}$C. This component is also present in the polyethylene results, but its relative contribution is significantly reduced. The extra component obtained with the polyethylene target is consistent with the solid curve (scattering off hydrogen), but only the kinematic solutions with the largest parallel velocities are populated. Both the hydrogen and carbon kinematic solutions overlap near $\theta = 0^\circ$ and thus it is not possible to completely separate the two polyethylene components using kinematics.

The presence of inelastic scattering from hydrogen can be confirmed by observing the recoil target protons. Figure 5(a) shows the distribution of $\Delta\phi$, the difference in azimuthal angles between the reconstructed parent $^{12}$Be fragment and a proton detected in the recoil-proton detectors. The observed yield obtained with the polyethylene target (histograms) is peaked at $\Delta\phi = \pm 180^\circ$ as expected for a recoil proton. The contribution from the carbon component of the target was determined with the carbon target and scaled to account for the relative carbon content and beam currents used with the two targets. This contribution is displayed as the connected lines and is essentially insignificant for all $\Delta\phi$ values. The resolution associated with $\Delta\phi$ is governed mostly by the size of the beam spot.

From the relative energies of the $\alpha$-$^{8}$He pair and the breakup $Q$-value, a reconstructed excitation energy $E^*$ of the parent $^{12}$Be fragment is determined. In addition, from the reconstructed parent velocity, a $Q$-value associated with the initial binary interaction is deduced. Two $Q$-values are determined for each event, $Q_C$ and $Q_H$, calculated assuming an interaction with a carbon or hydrogen target nucleus, respectively. For interactions with hydrogen we expect $Q_H = -E^*$. Figure 6(a) displays the distribution of $Q_H + E^*$. The results obtained with the polyethylene target has a peak at $Q_H + E^* = 0$ consistent with scattering off of hydrogen, but some of this yield is also from carbon scattering. The estimated contribution from these latter events, obtained with the carbon target, is also shown and it too displays a small peak at the same location. For the carbon target, the distribution of $Q_C + 1.4 \times E^*$ is displayed in Fig. 6(b). The factor 1.4 was

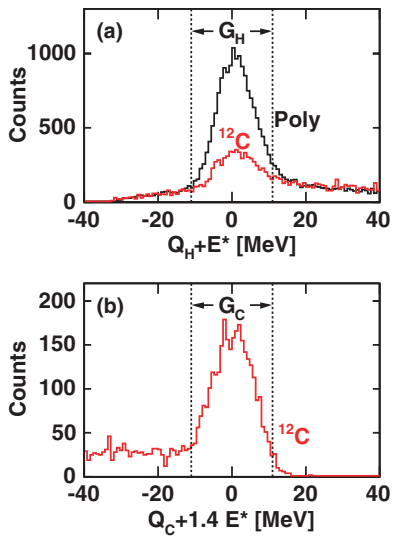


FIG. 6. (Color online) (a) Distributions of the sum of the $Q$-value, determined assuming an interaction with a hydrogen target nucleus, and the $^{12}$Be excitation energy (reconstructed for $\alpha$-$^{8}$He pairs). Results are shown for the polyethylene (poly) target. The distribution obtained with the carbon ($^{12}$C) target indicates the background expected from the carbon contribution of the polyethylene target. (b) Distribution of the sum of the $Q$-value, determined assuming an interaction with a carbon target nucleus, and the reconstructed excitation energy scaled by 1.4. The latter factor accounts approximately for the excitation energy of the scattered $^{12}$C fragments.

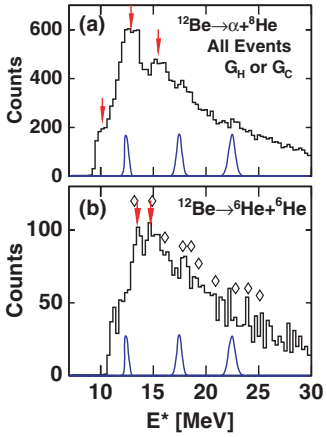


FIG. 7. (Color online) Distributions of excitation energy reconstructed from (a) $\alpha$-$^{8}$He and (b) $^{6}$He-$^{6}$He pairs. These experimental results are the sum of the contributions from both the polyethylene and carbon targets. The arrows indicate the locations of the structures discussed in the text. The diamonds indicate the locations of peaks identified in Ref. [10]. Examples of the predicted experimental response at three different excitation energies are indicated by the curves along the $E^*$ axis.

introduced to put the peak at zero energy. This implies that the scattered $^{12}$C fragment has, on average, 40% of the excitation energy of the $^{12}$Be fragment.

The vertical dashed lines in Figs. 6(a) and 6(b), indicate the gates $G_H$ and $G_C$ used to select events. The gate $G_H$ indicates the event is consistent with hydrogen scattering while $G_C$ is consistent with carbon scattering. Figure 7(a) shows the reconstructed excitation-energy distribution obtained from both targets. It includes events in the $G_H$ and $G_C$ gates for the polyethylene target and in the $G_C$ gate for the carbon target. Two broad flat-topped peaks at $E^* = 12.8$ and 15.5 MeV (indicated by the arrows) are visible. The widths

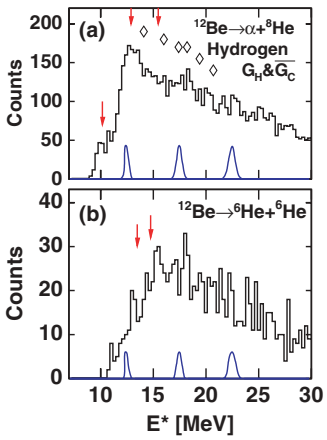


FIG. 8. (Color online) Distributions of excitation energy reconstructed from (a) $\alpha$-$^{8}$He and (b) $^{6}$He-$^{6}$He pairs for interactions on the hydrogen component of the polyethylene target. The arrows indicate the locations of the structures discussed in the text. The diamonds indicate the locations of peaks identified in Ref. [10]. Examples of the predicted experimental response are indicated by the curves along the $E^*$ axis.

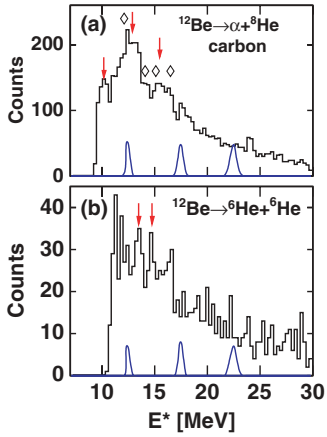


FIG. 9. (Color online) As for Fig. 8, but now the events are associated with scattering from $^{12}$C target nuclei. The data consist of the $G_C$-gated events obtained the carbon target and the $G_C$&$\overline{G_H}$-gated events obtained with the polyethylene target.

of these structures (~1.5 MeV) are significantly larger than the experimental resolutions of FWHM = 340 and 440 keV at these two energies. The square flat-topped shapes of these two structures indicate they cannot be associated with a single state (with a Lorentzian shape), but rather they are doublets, or possibly even higher order multiplets. In addition to the broad structures, a wide, low-energy shoulder at ~10.2 MeV is evident.

To investigate the target-nucleus dependence of these structures, the events were subdivided. The cleanest sample of events associated with hydrogen scattering was obtained with a $G_H$&$\overline{G_C}$ gate on the polyethylene events. The $E^*$ distribution associated with these events is shown in Fig. 8(a). This distribution is similar to the original distribution, except the doublet at $E^* = 15.5$ MeV is not evident. However, the $G_H$&$\overline{G_C}$ gate removes the most forward-angle events so it is possible that this doublet is still excited by hydrogen scattering.

A clean sample of carbon-scattering events is obtain from the $G_C$-gated carbon target events plus the $G_C$&$\overline{G_H}$-gated polyethylene events. The extracted $E^*$ distribution from this compound gate is displayed in Fig. 9(a). Both doublets are present, but the statistical significance of the higher-energy one is diminished. The relative yield in the low-energy shoulder (~10.2 MeV) has been significantly enhanced. From Figs. 8(a) and 9(a), we conclude that the 10.2 MeV low-energy shoulder and the 12.8 MeV doublet are excited from both hydrogen and carbon scattering. The origin of the higher-energy doublet is less clear.

From the Monte Carlo simulations we estimate the efficiencies for detecting the $\alpha$-$^{8}$He pair to be around 16% for both $^{12}$C and $^{1}$H target nuclei. From these efficiencies we determined the total cross sections for $\alpha$-$^{8}$He breakup listed in Table II. This table also includes cross sections for the other breakup channels studied in this work.

The work of Freer *et al.* [10] identified a number of peaks in equivalent distributions gated on hydrogen and carbon scattering. The locations of the peaks tabulated by Freer *et al.* are indicated by the diamonds in Figs. 8(a) and 9(a). However, neither of these spectra closely resemble those of

TABLE II. Breakup cross sections in mb for the exit channels measured from this work at a beam energy of $E/A = 50$ MeV and from Refs. [21] and [10] at $E/A = 42$ and 31 MeV, respectively.

| channel | target | This work $E/A = 50$ MeV | Ref. [21] $E/A = 42$ MeV | Ref. [10] $E/A = 31$ MeV |
|---|---|---|---|---|
| $^6$He-$^6$He | $^{12}$C | $0.73 \pm 0.22$ | $0.23 \pm 0.02$ | $0.28 \pm 0.4$ |
| $^6$He-$^6$He | $^1$H | $0.55 \pm 0.11$ | | $0.41 \pm 0.03$ |
| $\alpha$-$^8$He | $^{12}$C | $4.19 \pm 1.2$ | $1.02 \pm 0.04$ | $0.79 \pm 0.07$ |
| $\alpha$-$^8$He | $^1$H | $3.55 \pm 0.71$ | | |
| $t$-$^9$Li | $^1$H | $4.7 \pm 1.4$ | | |
| $p$-$^{11}$Li | $^1$H | $0.48 \pm 0.14$ | | |

Freer *et al*. The doublets, suggested in the present work, were not observed, though some of the listed peaks energies could be consistent with being one member of these doublet states.

### B. $^6$He+$^6$He decay

The velocity distributions for $^{12}$Be fragments reconstructed from $^6$He-$^6$He pairs is quite similar to the $\alpha$-$^8$He results and are not shown. The $\Delta\phi$ distribution in Fig. 5(b) confirms the presence of recoil protons from the polyethylene target. Excitation-energy spectra for all events and those associated with hydrogen and carbon scattering are displayed in Figs. 7(b), 8(b), and 9(b), respectively. Statistical fluctuations are too large in the latter two spectra to make any meaningful peak assignments. In the $E^*$ spectra for all events in Fig. 7(b), there is evidence for peaks at 13.5 and ~14.5 MeV (indicated by the arrows). However these peaks are rather small in magnitude and sit on a large "background" distribution.

Freer *et al*. have also identified a number of peaks from their combined $^{12}$C and $(CH_2)_n$ data for the $^6$He-$^6$He exit channel. The locations of these peaks are indicated in Fig. 7(b) by the diamonds. The lowest-energy peak at 13.2 MeV identified by Freer *et al*. is consistent with our 13.5 MeV peak. Freer *et al*. associated this peak with spin 4, based on angular correlations of the $^6$He fragments [11]. Due to the low signal-to-background ratio in the present work, we could not confirm this assignment. The second listed peak of Freer *et al*. at 14.9 MeV may be consistent with our ~14.5 MeV peak.

### C. $t$+$^9$Li decay

Significant yield was also observed for $t + {}^9$Li coincidences. The joint velocity distributions in Fig. 10(a) obtained with the polyethylene target indicate that the majority of these events have the kinematics associated with hydrogen scattering. Compared to the $^6$He-$^6$He and $\alpha$-$^8$He results, the angular distribution of the scattered Be fragments extends to much larger center-of-mass angles. The scattered recoil protons were again evident in the $\Delta\phi$ distribution of Fig. 5(c). The reconstructed excitation-energy distribution, determined from the polyethylene target and with the $G_H$ gate, is displayed in Fig. 10(b). This distribution has no prominent narrow peaks of statistical significance except for the suggestion of a peak at $E^* = 17.7$ MeV with a width similar to the experimental resolution.

### D. $p$+$^{11}$Li decay

A small number of $p$-$^{11}$Li pairs were detected. The joint velocity distributions in Fig. 11(a) obtained with the polyethylene target again indicate that the parent fragments were excited by interactions with hydrogen target nuclei. The detection efficiency for small $V_\perp$ is suppressed due to the angular acceptance of the heavy $^{11}$Li fragment, which essentially defines the center of mass. Otherwise, the reconstructed parents uniformly occupy the full range of center-of-mass angles. Due to the difficultly is detecting the $^{11}$Li fragments, the average detection efficiency was estimated to be only 4%

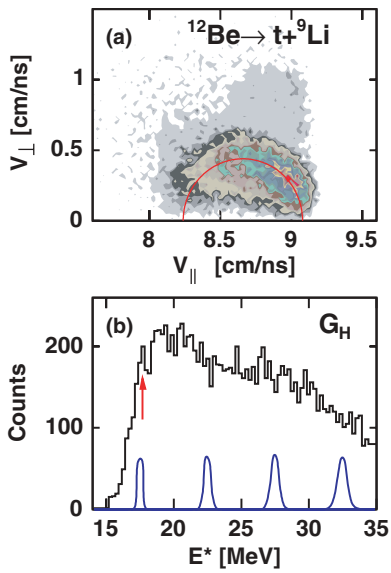


FIG. 10. (Color online) Results obtained for $^{12}$Be fragments reconstructed from $t$-$^9$Li pairs. (a) The joint distribution of parallel and perpendicular velocities. The circular curve indicates the kinematic solution expected for inelastic scattering from a hydrogen target nucleus exciting the $^{12}$Be to 28 MeV of excitation energy. (b) The reconstructed excitation-energy distribution of the $^{12}$Be fragments for events in the $G_H$ gate. Examples of the predicted experimental response are indicated by the curves along the $E^*$ axis. The arrow indicates the location of the structure discussed in the text.

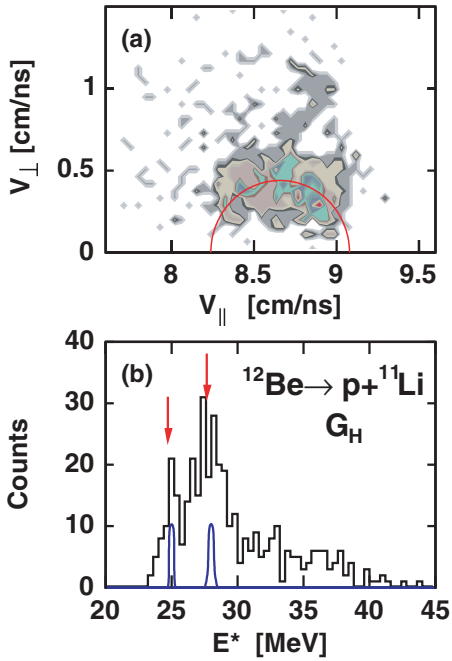


FIG. 11. (Color online) Results obtained for $^{12}$Be fragments reconstructed from $p$-$^{11}$Li pairs. (a) The joint distribution of parallel and perpendicular velocities. The circular curve indicates the kinematic solution expected for inelastic scattering from a hydrogen target nucleus exciting the $^{12}$Be to 28 MeV of excitation energy. (b) The reconstructed excitation-energy distribution of the $^{12}$Be fragments for events in the $G_H$ gate. Examples of the predicted experimental response are indicated by the curves along the $E^*$ axis. The arrows indicate the locations of the structures discussed in the text.

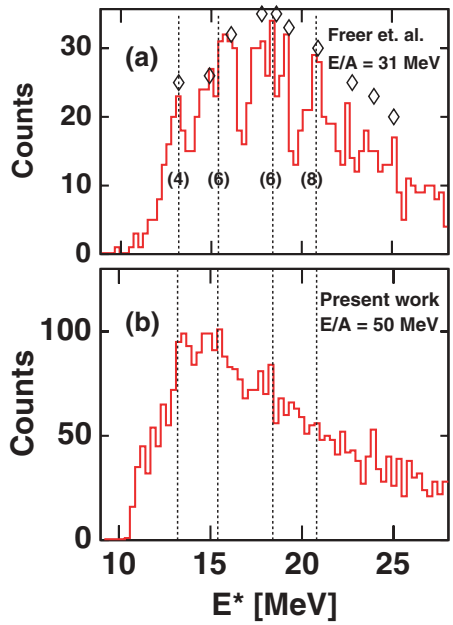


FIG. 12. (Color online) Comparison of the spectra of excitation energy for the $^6$He-$^6$He channel obtained from (a) Ref. [11] to (b) the results of this work. In both spectra, events produced from interactions with hydrogen and carbon target nuclei are included. The vertical dashed lines indicate the approximate centroids of the four large structures for which spin assignments were made by Freer *et al.* Individual peak locations listed by these authors are indicated by the diamond symbols. The numbers in parenthesis are the assigned spins.

in the Monte Carlo simulations. As for the other channels, the $\Delta\phi$ distribution of Fig. 5(d) confirms the presence of recoil protons. The reconstructed excitation-energy distribution from the polyethylene target and with the $G_H$ gate, shown in Fig. 11(b), has some prominent and significant features. Most notable is a wide peak at $E^* = 28$ MeV of width 2.7 MeV. This is significantly larger than the experimental resolution of FWHM = 370 keV. From the statistical fluctuations, it is difficult to say whether this structure is a single peak or a multiplet. There is also a clear indication of a narrow peak at $E^* = 25$ MeV. Its width is similar to the predicted experimental resolution.

## V. DISCUSSION AND CONCLUSIONS

It is important to examine to what extent the results of this work are consistent with those of Freer *et al.* [10,11] obtained at the lower bombarding energy of $E/A = 31$ MeV. In Secs. IV A and IV B we indicated that many of the possible states listed by Freer *et al.* for $^6$He-$^6$He and $\alpha$-$^8$He decay were not observed with clear statistical significance in this work. Figure 12 shows a direct comparison of the $^6$He-$^6$He spectra (comprising breakup from both hydrogen and carbon target nuclei) obtained by Freer *et al.* to that from this work. The number of detected $^6$He-$^6$He and $\alpha$-$^8$He pairs in the present work is significantly larger, while our excitation-energy resolution is comparable to that of Freer *et al.* They quote an excitation-energy resolution of FWHM = 800 keV for $10 < E^* < 25$ MeV [11]. Over the same range, our Monte Carlo simulations (Sec. III) predict the resolution changes from 250 to 800 keV.

They list a total of ten possible $^6$He+$^6$He breakup states. However of most statistical significance are four structures (some wide) located at 13.3, 15.5, 18.5, and 21 MeV (indicated by the dashed lines in Fig. 12) for which spin assignments were made. From these spin assignments, a rotational structure with large moment of inertia was inferred and thus it was concluded there was strong evidence for an exotic $^6$He+$^6$He molecular structure which may be based on an $\alpha$-4$n$-$\alpha$ cluster configuration.

In comparison with the results of Freer *et al.*, our $^6$He-$^6$He spectrum, shown in Fig. 12, is remarkably structureless. However the closer examination offered in Sec. IV B suggests some small peaks on a large "background". The first of these at 13.5 MeV may possibly be associated with the 13.2 MeV peak of Freer *et al.* which was assigned a spin of 4, although this peak does seem to be shifted to a slightly higher energy. We also tentatively identify a small peak at 14.5 MeV which might be associated with the wider structure of Freer *et al.* at 15.5 MeV which was assigned at spin of 6. Identification of the 18.5 and 21 MeV structures which were assigned spins of 6 and 8, respectively by Freer *et al.* are tenuous at best and not statistically significant. Given that we have problems identifying all the structures, let along making spin assignments, we are not able to confirm the presence of $^6$He-$^6$He rotational structure in $^{12}$Be. If these

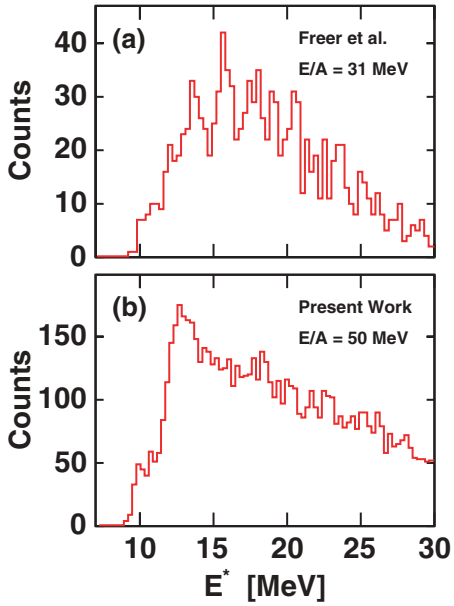


FIG. 13. (Color online) Comparison of the spectra of excitation energy for the $\alpha$-$^{8}$He channel after interactions with hydrogen target nuclei obtained from (a) Ref. [11] to (b) the results of this work.

structures are real, then they are excited relatively weakly compared to the "background" at the higher bombarding energy ($E/A = 50$ MeV) of this work.

Comparisons are also made of excitation-energy distributions for the $\alpha + {}^{8}$He channel in Figs. 13 and 14 for interactions on hydrogen and carbon target nuclei, respectively. Again the spectra obtain by Freer *et al.* and the present work are quite different. A large number of the peaks obtained by Freer *et al.* do not have statistical significant counterparts in the spectra from this work.

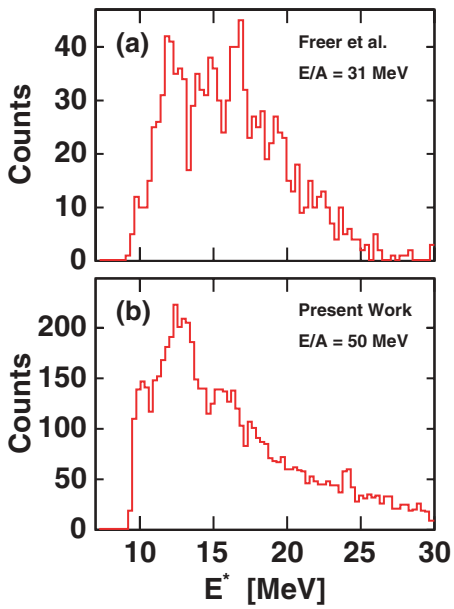


FIG. 14. (Color online) Comparison of the spectra of excitation energy for the $\alpha$-$^{8}$He channel after interactions with carbon target nuclei obtained from (a) Ref. [11] to (b) the results of this work.

The origin of the "background" is not clear. Both the $^{6}$He-$^{6}$He and $t$-$^{9}$Li channels are dominated by this background and it is still relatively substantial for the $\alpha$-$^{8}$He channel. For all channels, the background events have consistent kinematics and reconstructed excitation energies and thus correspond to real projectile-breakup events. Because of the high thresholds for the detected channels, we are exploring states at high excitation energy where the density of states, as well as the typical widths, are expected to be large. Is it possible that the background could be associated with the summation of these unresolved states? The states are all well above the neutron decay threshold (Table I) and therefore we may expect large widths due to neutron emission, useless the nuclear structure of the levels hinder such decays. In particular, states with strong cluster structure are expected to suppress neutron decay and select out decay modes with similar cluster structure. Thus the $^{6}$He-$^{6}$He and $\alpha$-$^{8}$He channels are expected to preferentially enhance these cluster states. Given the rather structureless nature of the observed $^{6}$He-$^{6}$He spectra it is clear that this expectation is not met or alternatively some other source of background is present. One possibility is that an intermediate excited state is not produced, but the breakup is direct via interaction with the target's Coulomb or nuclear field. While direct breakup reactions are well known in this energy regime [22,23], in order to populate cluster decay modes, the ground-state itself should have an admixture with cluster structure. If the magnitude of the direct component increases significantly with bombarding energy, then this could help explain the disappearance of the structures observed at $E/A = 31$ MeV by Freer *et al.* at the higher bombarding energy of this work. Such a scenario may be indicated by an increased $^{6}$He-$^{6}$He total cross section at $E/A = 50$ MeV.

To investigate this possibility, total cross sections for observed exit channels of this work are compared to results at $E/A = 31$ MeV from Freer *et al.* [10] and at $E/A = 42$ MeV from Ashwood *et al.* [21] in Table II. For the $^{6}$He-$^{6}$He exit channel formed in interactions with hydrogen target nuclei, there are only results for $E/A = 31$ and the present study ($E/A = 50$ MeV). The two cross sections are identical within the experimental errors. However for the $^{12}$C target, there is a significant difference in the cross sections at these two energies, the higher energy value is approximately 2.5 times larger. However at the intermediate bombarding energy ($E/A = 42$ MeV), the cross section is consistent with the $E/A = 31$ MeV value. This would point to a rather unusual bombarding-energy dependence or alternatively may signify that the differences in cross sections are artifacts of the assumptions employed in the analysis of the three different studies. The $\alpha$-$^{8}$He cross sections for the $^{12}$C target show a similar trend. Given our difficulty in understanding the energy dependence of these cross sections, we can made no strong statement as to whether the background of this work has increased in absolute sense from that found at the lower energy by Freer *et al.*

This work has some consistency with other previous studies. For instance, our $\sim$10.2 MeV $\alpha$-$^{8}$He state maybe related to the 10 MeV state of Korsheninnikov *et al.* [9] and/or the 10.7 MeV state of Bohlen *et al.* [14]. Similarly our $\sim$14.5 MeV $^{6}$He-$^{6}$He state maybe related to the $\sim$14 MeV

state of Korsheninnikov *et al*.and the 14.6 MeV state of Bohlen *et al*.

In comparing the structure observed in the two helium decay channels, it is important to realize that the $\alpha$-$^{8}$He decay channel can be accessed by states of both parities, while only positive-parity states can decay by the symmetric $^{6}$He-$^{6}$He breakup. The 13.5 MeV peak in the $^{6}$He-$^{6}$He distribution may be the upper member of the 12.8 MeV doublet observed for $\alpha$-$^{8}$He events. The absence of the lower member of this doublet in the $^{6}$He-$^{6}$He channel, suggests that lower state has negative parity. The doublet would then have negative and positive party states. In the work of Freer *et al*., the upper state was assigned a spin of $4^{+}$ [11]. Using the Generator Coordinate Method for just the $\alpha$-$^{8}$He molecular configurations, Descouvemont and Baye predict doublets each containing a member of a positive and a negative parity molecular band [8]. They even predict a $(5^{-}, 4^{+})$ doublet very close to our observed 12.8 MeV doublet. However when they allow mixing with $^{6}$He-$^{6}$He molecular configurations, the ordering of the doublet is reversed. The 12.8 MeV shoulder structure in the $\alpha$-$^{8}$He spectra could be the lower $(3^{-}, 2^{+})$ members of these molecular bands. However, the upper 15.5 MeV doublet is too low in energy to be the $(7^{-}, 6^{+})$ members. Therefore, the exact nature of all the observed states is unclear.

Of particular interest is the magnitude of the $t$-$^{9}$Li channel, it is the strongest of all the exit channels produced in interactions on hydrogen target nuclei (Table II). Given that one generally does not expect states with strong triton structure, either excited state for resonant decay or in the ground state for direct decay, the origin of this component is not clear and especially its strong dependence on target nuclei.

In contrast to the other channels, the $p$-$^{11}$Li channels has the most prominent structure (Fig. 11). Given the discussion on the background it is clear that these states, which are probably more shell-model-like in nature, cannot have strong neutron branching ratios. The 25 MeV state maybe the isobaric analog of the particle-unstable $^{12}$Li ground state in which case isospin conservation would suppress neutron decay. The $^{12}$Li ground state has not been observed experimentally, but based on the estimated mass excess of 50.1±1.0 MeV [24] and the measured Coulomb displacement energy of $\Delta E_c =$ 1.32±0.02 MeV for isobaric analog of $^{11}$Li [25], we estimate an excitation energy of 25.5±1.0 MeV for the isobaric analog state in $^{12}$Be. This is consistent with the location of the observed peak. The higher-lying structure around 28 MeV of excitation energy could correspond to excited analog states of $^{12}$Li.

In conclusion, $\alpha$+$^{8}$He, $^{6}$He+$^{6}$He, $t$+$^{9}$Li, and $p$+$^{11}$Li decays of $^{12}$Be fragments excited via inelastic scattering with hydrogen and carbon target nuclei have been observed. Events were isolated where the $Q$-value associated with the initial primary inelastic-scattering interaction and the excitation energy determined from the relative energy of the secondary decay fragments were consistent. The $\alpha$+$^{8}$He and $^{6}$He+$^{6}$He decays have significant contributions from both $^{12}$C and $p$ scattering, while the $t$+$^{9}$Li and $p$+$^{11}$Li channels were produced predominantly through $p$ scattering. For $\alpha$+$^{8}$He decay, two doublets were observed at 12.2 and 15.5 MeV of excitation energy and the presence of additional state(s) is indicated by a shoulder in the spectrum at 10.2 MeV. Freer *et al*. [11] report evidence for $^{6}$He-$^{6}$He rotational structures in $^{12}$Be which maybe based on an $\alpha$-4$n$-$\alpha$ cluster configuration. Apart from the suggestion of peaks at 13.5 and 14.5 MeV for $^{6}$He-$^{6}$He decay we were not able to confirm this result. The $p$+$^{11}$Li channel was found to display a narrow peak at 25 MeV and a broad structure at 28 MeV possibly associated with $T = 3$ analog states.

## ACKNOWLEDGMENTS

This work was supported by the U.S. Department of Energy, Division of Nuclear Physics under grants DE-FG02-87ER-40316 and DE-FG02-04ER41320 and the National Science Foundation under grants PHY-0606007 and PHY-9977707.

[1] M. Freer and A. C. Merchant, J. Phys. G **23**, 261 (1997).
[2] S. Okabe, Y. Abe, and H. Tanaka, Prog. Theor. Phys. **57**, 866 (1977).
[3] W. von Oertzen, Z. Phys. A **354**, 37 (1996).
[4] W. von Oertzen, Z. Phys. A **357**, 355 (1997).
[5] Y. Kanada-En'yo and H. Horiouchi, Prog. Theor. Phys. Suppl. **142**, 205 (2001).
[6] M. Freer, E. Casarejos, L. Achouri, C. Angulo, N. I. Ashwood, N. Curtis, P. Demaret, C. Harlin, B. Laurent, M. Milin *et al*., Phys. Rev. Lett. **96**, 042501 (2006).
[7] M. Ito and Y. Sakuragi, Phys. Rev. C **62**, 064310 (2000).
[8] P. Descouvemont and D. Baye, Phys. Lett. **B505**, 71 (2001).
[9] A. A. Korsheninnikov, E. Y. Nikolskii, T. Kobayashi, D. V. Aleksandrov, Fujimaki, H. Kumagai, A. A. Oglobin, A. Ozawa, I. Tanihata, Y. Watanabe *et al*., Phys. Lett. **B343**, 53 (1995).
[10] M. Freer, J. C. Angélique, L. Axelsson, B. Benoit, U. Bergmann, W. N. Catford, S. P. G. Chappell, N. M. Clarke, N. Curtis, A. D'Arrigo *et al*., Phys. Rev. C **63**, 034301 (2001).
[11] M. Freer, J. C. Angélique, L. Axelsson, B. Benoit, U. Bergmann, W. N. Catford, S. P. G. Chappell, N. M. Clarke, N. Curtis, A. D'Arrigo *et al*., Phys. Rev. Lett. **82**, 1383 (1999).
[12] A. Saito, S. Shimoura, S. Takeuchi, T. Motobayashi, T. Minemura, Y. U. Matsuyama, H. Baba, H. Akiyoshi, Y. Ando, N. Aoi *et al*., Nucl. Phys. **A738**, 337 (2004).
[13] A. Saito, S. Shimoura, S. Takeuchi, T. Motobayashi, H. Akiyoshi, Y. Ando, N. Aoi, Z. Fülöp, T. Gomi, Y. Higurashi *et al*., Prog. Theor. Phys. (Kyoto), Suppl. **146**, 615 (2002).
[14] H. G. Bohlen, W. von Oertzen, A. Blažević, B. Gebauer, S. M. Grimes, R. Kalpakchieva, T. N. Massey, and S. Thummerer, Phys. At. Nucl. **65**, 635 (2002).
[15] N. Curtis, N. I. Ashwood, L. T. Baby, T. D. Baldwin, T. R. Bloxham, W. N. Catford, D. D. Caussyn, M. Freer, C. W. Harlin, P. McEwan *et al*., Phys. Rev. C **73**, 057301 (2006).
[16] M. S. Wallace, M. A. Famiano, M.-J. van Goethem, A. M. Rogers, W. G. Lynch, J. Clifford, F. Delaunay, J. Lee, S. Labostov, M. Mocko, L. Morris, A. Moroni, B. E. Nett, D. J. Oostdyk, R. Krishnasamy, M. B. Tsang,

R. T. de Souza, S. Hudan, L. G. Sobotka, R. J. Charity, J. Elson, and G. L. Engel, Nucl. Instrum. Methods Phys. Res. A **583**, 302 (2007).

[17] G. L. Engel, M. Sadasivam, M. Nethi, J. M. Elson, L. G. Sobotka, and R. J. Charity, Nucl. Instrum. Methods Phys. Res. A **573**, 418 (2007).

[18] B. Davin, R. D. de Souza, R. Yanez, H. S. X. Y. Larochelle Amd, R. Alfaro, A. Alexander, K. Bastin, L. Beaulieu, J. Dorsett, G. Fleener, L. Gelovani *et al*., Nucl. Instrum. Methods Phys. Res. A **473**, 302 (2001).

[19] J. F. Ziegler, J. P. Biersack, and U. Littmark, *The Stopping and Range of Ions in Solids* (Pergamon Press, New York, 1985), the code SRIM can be found at www.srim.org.

[20] R. Anne, J. Herault, R. Bimbot, H. Gauvin, G. Bastin, and F. Hubert, Nucl. Instrum. Methods B **34**, 295 (1988).

[21] N. I. Ashwood, M. Freer, S. Ahmed, J. C. Angélique, V. Bouchat, W. N. Catford, N. M. Clarke, N. Curtis, O. Dorvaux, B. R. Fulton *et al*., Phys. Lett. **B580**, 129 (2004).

[22] K. Ieki, D. Sackett, A. Galonsky, C. A. Bertulani, J. J. Kruse, W. G. Lynch, D. J. Morrissey, N. A. Orr, H. Schulz, B. M. Sherrill *et al*., Phys. Rev. Lett. **70**, 730 (1993).

[23] R. J. Charity, L. G. Sobotka, N. J. Robertson, D. G. Sarantites, J. Dinius, C. K. Gelbke, T. Glasmacher, D. O. Handzy, W. C. Hsi, M. J. Huang *et al*., Phys. Rev. C **52**, 3126 (1995).

[24] G. Audi, A. H. Wapstra, and C. Thibault, Nucl. Phys. **A729**, 337 (2003).

[25] T. Teranishi, S. Shimoura, Y. Ando, M. Hirai, N. Iwasa, T. Kikuchi, S. Moriya, T. Motobayashi, H. Murakami, T. Nakamura *et al*., Phys. Lett. **B407**, 110 (1997).